11th International Symposium on Turbulence and Shear Flow Phenomena (TSFP11)
Southampton, UK, July 30 to August 2, 2019

FORMATION AND EVOLUTION OF SHEAR LAYERS IN A DEVELOPING TURBULENT BOUNDARY LAYER

J. H. Lee*, **N. Hutchins and J. P. Monty**
Department of Mechanical Engineeing
The University of Melbourne, Victoria 3010, Australia
*email: jung.lee@unimelb.edu.au

M. Kozul
Department of Energy and Process Engineering
Norwegian University of Science and Technology, Gløshaugen, No-7491 Trodheim, Norway

ABSTRACT

The evolution and formation mechanism of large-scale shear layers in a turbulent boundary layer are investigated using time-resolved PIV datasets of a developing turbulent boundary layer from inception at the trip up to a friction Reynolds number of Re_τ =3000. The spatially developing boundary layer is formed on a 5m long flat plate towed through a water tank. In this frame of reference, evolving large-scale features with convection velocities close to the freestream appear nominally stationary within the field of view, enabling us to track the development of these features. An analysis of the instantaneous convection velocity associated with low- and high-speed motions reveals that there are differences in the trajectory and local convection velocity between these large-scale motions at a given wall-height in the outer region. As these motions travel at different speeds, a sequence of instantaneous streamwise velocity fluctuation fields shows that strong streamwise velocity gradients appear along the interfaces where low- and high-speed regions interact. To further investigate how these regions are associated with the formation of shear layers in a turbulent boundary layer, we compute conditional averages of streamwise velocity fluctuation based on strong shear layers. The results suggest that the difference in convection velocities between low- and high-speed regions can cause these regions to come together, forming internal shear layers in the outer layer. In addition, a sequence of instantaneous velocity fluctuation fields exhibit signs of shear layer roll-up following the formation of these shear layers, leading to the development of a large-scale slowly overturning motion. Based on these findings, we discuss a conceptual scenario which describes dynamic interactions of these shear layers and their associated large-scale coherent motions.

Introduction

Over the past few decades, significant research effort has attempted to understand and describe recurrent flow patterns, known as coherent structures, in turbulent boundary layers. One distinct feature often reported is the persistent presence of shear layers, which are mostly associated with strong gradients (both axial and wall-normal) of the streamwise velocity component. For example, Robinson (1991) reported the occurrence of thin shear layers throughout a turbulent boundary layer at the interfaces between upstream high-speed regions and downstream low-speed regions. Robinson (1991) mainly observed this phenomenon near the wall, where instability arguments are commonly invoked to explain the origin of vortices (Kline *et al.*, 1967; Corino & Brodkey, 1969; Kim *et al.*, 1971). Flow visualisation studies of Kline *et al.* (1967) also suggested that the ejection event could be due to a local instability mechanism and seem to play a key role in the transport of turbulent kinetic energy away from the wall. Further to this, Kim *et al.* (1971) and Willmarth & Lu (1972) proposed that inflectional behaviour in instantaneous velocity profiles associated with these shear layers eventually leads to vortex formation through a local shear instability. Intense shear layers are also known to demarcate two large regions with nearly uniform streamwise momentum (Adrian *et al.*, 2000; de Silva *et al.*, 2016). This behaviour is prevalent not only instantaneously but is also persistent enough to appear in the linear stochastic estimation (Christensen & Adrian, 2001).

While the existence and the importance of shear layers within turbulent boundary layers are relatively well-documented, the dynamics of these coherent features are yet to be rigorously examined. One important dynamical property of these large-scale motion is how they convect and evolve in time and space. Despite the considerable attention this subject has received (Krogstad *et al.*, 1998; Gao *et al.*, 2011; Lee *et al.*, 2014*a*; Lozano-Durán & Jiménez, 2014), the local convection velocity of the coherent motions still remains a controversial subject. It is common practice to use Taylor's hypothesis of frozen flow with a local mean streamwise velocity (Hutchins & Marusic, 2007) to convert temporal data from experiments into a spatial domain. Previously, it has been shown that the convection velocity is related to the scale of structures (del Álamo & Jiménez, 2009; Monty & Chong, 2009; Hutchins *et al.*, 2011). However, these studies provide only time-averaged mean statistics, while the local instantaneous convection velocity of individual features in turbulent boundary layers remains largely unknown. More recently, Lee *et al.* (2014*a*) used DNS data to individually track large-scale structures while examining their spatial and temporal characteristics. One distinct feature reported in the study is how the convec-

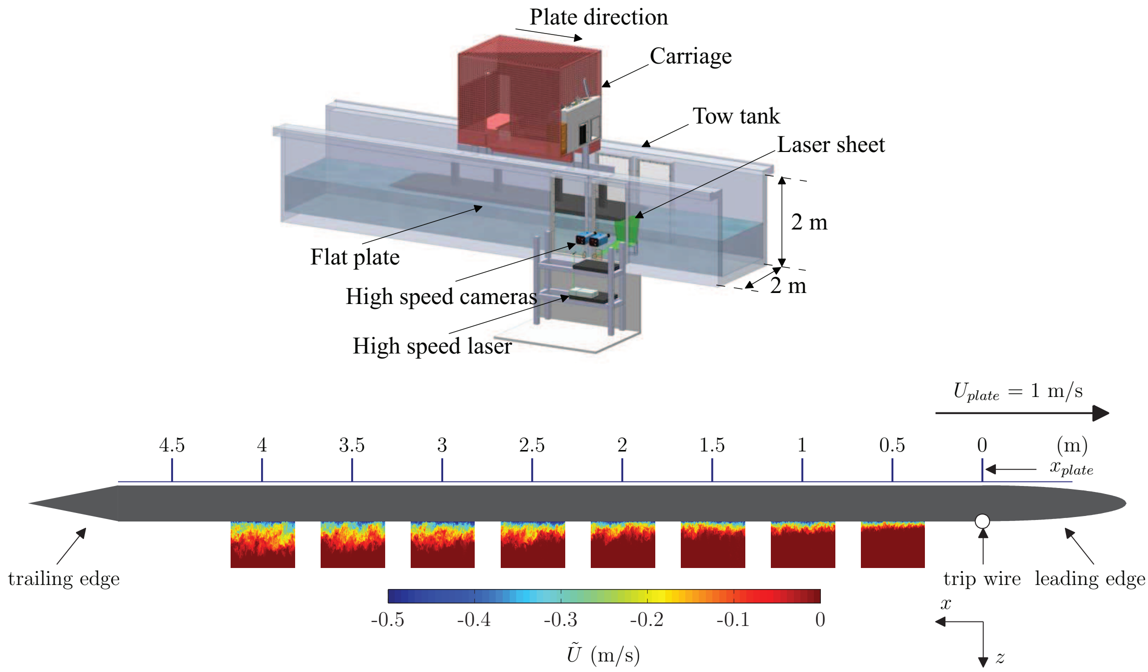

Figure 1. (a) Time-resolved PIV setup with plate in tow tank (b) Schematic of the plate with PIV captured developing boundary layer along the length of the plate

tion velocity can vary among the detected features even at a fixed wall distance. They found that positive and negative streamwise velocity fluctuations convect at distinguishably different speeds, suggesting that these differences played a crucial role in the formation of very-large-scale structures. Further to this, Lozano-Durán & Jiménez (2014) and de Kat & Ganapathisubramani (2015) have also shown that the ejection-like (Q2) events convect slower in the streamwise direction than the sweep-like (Q4) events by tracking individual events using temporally resolved DNS and particle image velocimetry (PIV) data of wall-bounded turbulent flows respectively.

Although many of these investigations have shed new light on the dynamical features of the coherent structures, the origin, lifespan and development of these large-scale regions and shear layers still remain largely unresolved. Hence in the current study, we attempt to further examine the dynamical features and associated formation mechanism of the shear layers in an evolving turbulent boundary layer using a temporally resolved PIV database. These experiments take advantage of the towed-plate coupled with a stationary time-resolved PIV (TRPIV) system such that the evolving large-scale features can be tracked over many boundary layer turnover times.

Description of experiments

The experiments are performed in the tow tank facility located in the Michell hydrodynamics laboratory at the University of Melbourne. The tow tank has dimensions of 60 × 2 × 2 m (length × width × height) and is filled with water. As indicated in figure 1(a), the fully-automated traversing carriage tows a 5 m long and 1.2 m wide flat plate at a towing velocity of approximately 1.0 m/s ($U_{plate} \equiv U_\infty$ after Galilean transformation). Figure 1(b) shows examples of a boundary layer developing along the length of the plate captured using time-resolved PIV. A visual aid to demonstrate the towed plate experiment and a sequence of time-resolved instantaneous streamwise velocity fields of a developing turbulent boundary layer is available online[1]. Throughout this paper, x, y and z denote the streamwise, spanwise and wall-normal directions, with u, v and w denoting the respective fluctuating velocity components. Overbars indicate time-averaged quantities (e.g. $\overline{U}$). The superscript '+' is used to denote quantities normalised by viscous scaling for length ($z^+ = zU_\tau/\nu$), time ($t^+ = tU_\tau^2/\nu$) and velocities ($U^+ = U/U_\tau$).

Re_τ	δ (mm)	U_τ (ms^{-1})	l^+	Δt^+
700 - 3300	15 - 90	0.05 - 0.04	54 - 66	1.4 - 2.0

Table 1. Experimental parameters for TRPIV experiments. Ranges indicate the variation of parameters over the streamwise length of the plate $0 < x_{plate}$ (m) < 5 when U_{plate} = 1 m/s.

All images are acquired at a sampling rate of 1000 Hz which gives Δt = 1 ms (where Δt is the time between images). This equates to $\Delta t^+ \approx 1.7$ at $U_{plate} = 1$ m/s. A total of 122 runs, where each run is one complete tow of the plate past the measurement system, are performed. Two cameras are used to provide a measurement field of view of 170 mm × 80 mm ($x \times z$) and each run acquires 5000 images per camera covering the entire streamwise domain of the plate from the trip to the trailing edge. Experimental conditions are summarised in table 1, where x_{plate} is the streamwise distance downstream of the trip device. Further details on the experiments and the validation of the flows can be found in Lee *et al.* (2014*b*).

[1] http://dx.doi.org/10.1103/APS.DFD.2014.GFM.V0054

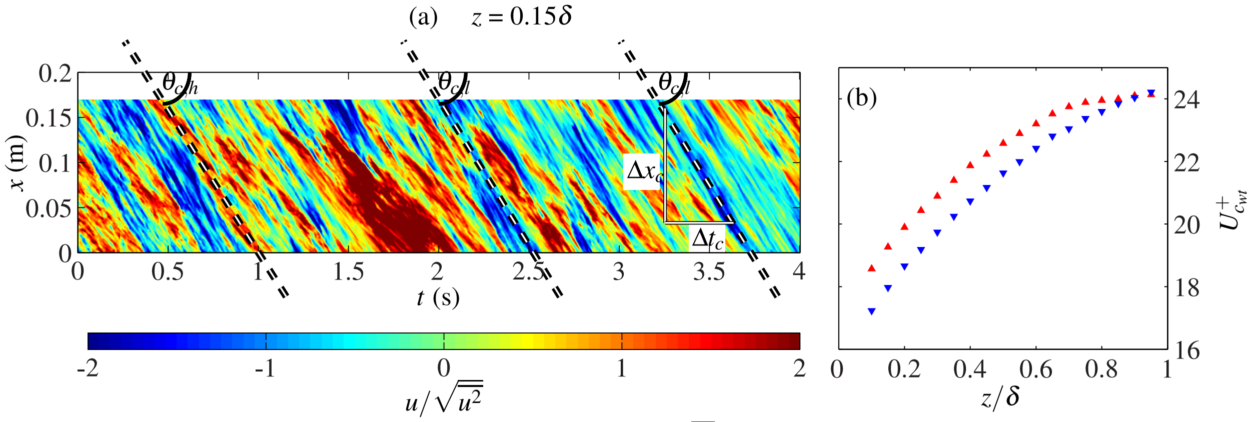

Figure 2. (a) Normalised streamwise fluctuating velocity field ($u/\sqrt{\overline{u^2}}$) at constant $z = 0.15\delta$ in $x-t$ plane. Dashed lines illustrate the inclination angle of stripy footprint. θ is the inclination angle. The subscript 'l' and 'h' denote quantities associated with the low- and high-speed regions, respectively. (b) Mean convection velocity $U^+_{c_{wt}}$ associated with low- (▼) and high-speed (▲) regions at different wall-normal positions from 0.1δ to δ shown at increments of 0.1δ.

Results

To extract the convection velocity of low- ($-u$) and high- ($+u$) speed regions, a space-time volume is constructed by stacking the sequence of instantaneous fields of the streamwise fluctuating velocity components in time creating an $x-z-t$ diagram. Figure 2(a) shows a sliced $x-t$ plane extracted at constant $z = 0.15\delta$, offering a unique view of the convecting instantaneous low- and high-speed regions. The $x-t$ plane is normalised with the local root mean square turbulent intensity values ($u/\sqrt{\overline{u^2}}_{local}$), where $\sqrt{\overline{u^2}}_{local}$ is a function of x and z. One of the distinct features in this planar view is the inclined stripy pattern as indicated by the dashed lines. These angled regions represent the streamwise trajectories of the turbulent features as they evolve in time and specifically, the inclination angle indicates the streamwise convection velocity of the corresponding features within the measurement field of view following $\tan(\theta_c) = \Delta x_c/\Delta t_c = U_c$, where θ_c is the inclination angle of a convecting structure and the subscript 'c' represents convection quantities. Δx_c is a streamwise distance that the structure convected in time, Δt_c. More extensive details on the feature detection scheme and associated validation can be found in Lee (2017). It is important to note that the convection velocity defined in this way is relative to the stationary field of view. In a wind tunnel frame of reference (where the flow is imposed over a stationary plate and observed with a fixed PIV system), the equivalent convection velocity is $U_{c_{wt}} = U_{\infty,wt} - U_c$ where the subscript 'wt' indicates the wind tunnel frame of reference. An advantage with the current towed plate experiment is that convecting structures can often be tracked throughout their entire evolution or life span. Figure 2(b) shows the mean convection velocity scaled with local viscous scaling for low- and high-speed regions as a function of the wall-normal position. The results are presented after applying the Galilean transformation to provide the wind tunnel frame of reference. The observed increasing convection velocity trend with wall height agrees with the observations of del Álamo & Jiménez (2009). Note that the discrepancy between the convection velocity associated with low- (▼) and high- (▲) speed regions at the same wall-position reduce with distance from the wall. This is consistent with the reduction in mean shear and turbulence intensity (Lee *et al.*, 2014*a*) with increasing wall heights. On a similar note, Krogstad *et al.* (1998) reported that the convection velocity for ejection events is lower than for sweep events at all scales throughout the boundary layer as also recently observed by Lozano-Durán & Jiménez (2014) and de Kat & Ganapathisubramani (2015). These results support the mismatched mean convection velocities in figure 2(b) since the ejection and sweep events are highly correlated with negative- and positive-u respectively.

Based on our observations for the mismatch in the convection velocities between these two regions, we attempt to investigate a mechanism for internal shear layer formation within turbulent boundary layers. Figures 3 (a-d) show a sequence of u^+ while the plots (e-h) show the associated dU^+/dz^+ for the same snapshots. In a time sequence, such as the one shown in figure 3, the mismatched convection velocities will cause the low-speed regions to 'catch up' or 'interact' with upstream high-speed regions. In figures 3(a-d), one can observe a low-speed region and a high-speed region (marked with an ellipse) in the middle of the field of view. As time progresses, this region increasingly catches up with the upstream high-speed region with an associated sharpening of the velocity gradient at the interface between the two regions. The corresponding dU^+/dz^+ sequence shown in figures 3(e-h) shows a strong inclined shear forming along this interface (marked with an ellipse). This observation suggests that the mismatched convection velocities between the low- and high-speed regions may offer a possible formation mechanism for the inclined shear layers that are commonly observed in the outer region of turbulent boundary layers.

In order to test this hypothesis, here we analyse the relationship between the mismatch in the convection velocity and the formation of the shear layer by computing spatial and temporal conditional quantities as follows. We define an internal shear layer as the region when the instantaneous $d\tilde{U}^+/dz^+$ is higher than the local mean $d\overline{U}^+/dz^+$. We then search, at a given condition location in z, for regions in the instantaneous velocity fluctuation field where $d\tilde{U}^+/dz^+$ is higher than the threshold. Having detected these regions, we then employ a lag and lead conditional averaging scheme as used by Chung *et al.* (2012). A similar approach called VISA (variable interval space averaging) was used in Johansson *et al.* (1991) to investigate space-time development of near-wall flow structures, where they tracked individual strong shear layer regions in time and space. With the lag and lead conditional averaging method, we can ensem-

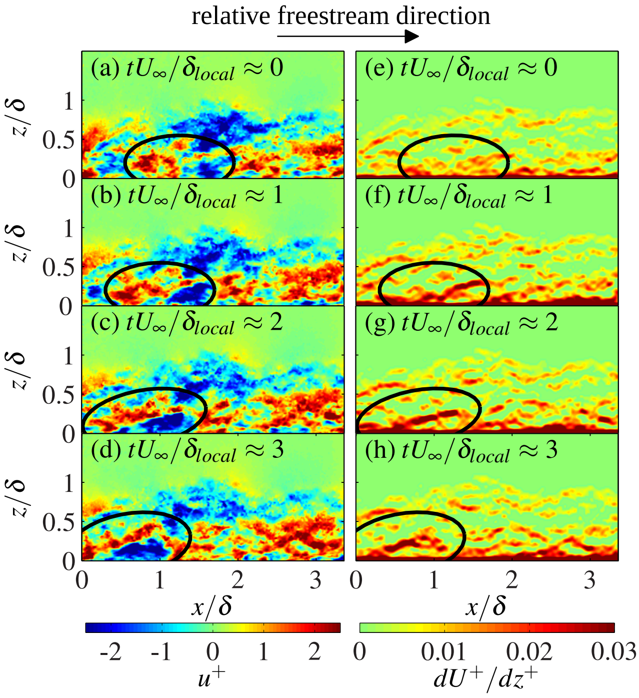

Figure 3. (a-d) sequence of the streamwise velocity fluctuation, u^+ and (e-h) the corresponding instantaneous wall-normal gradient of the streamwise velocity, dU^+/dz^+. Time separation between plots is $\Delta tU_\infty/\delta \approx 1$.

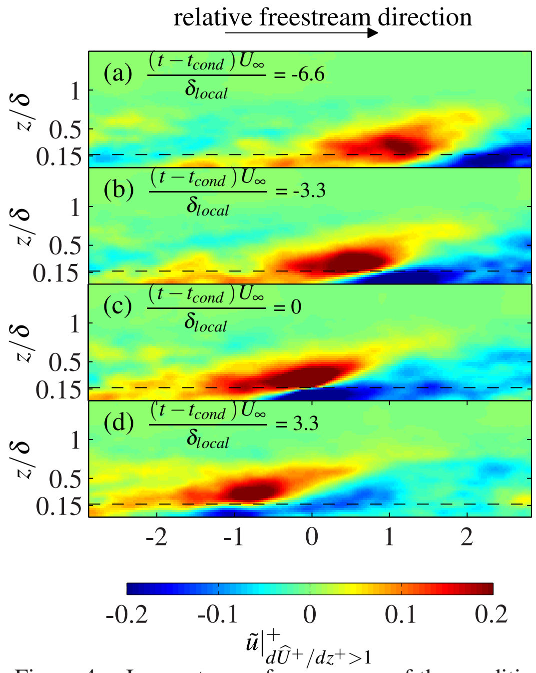

Figure 4. Iso-contours of a sequence of the conditionally averaged u^+ computed based on a strong shear layer event at $z/\delta = 0.15$ at $Re_\tau \approx 1400$. This sequence shows the prior and subsequent fields relative to the reference time.

ble a conditional sequence prior to and after the detected shear layer event. This in turn permits us to observe the spatio-temporal development of the shear layer formation and the related large-scale motion. Figure 4 shows a sequence of iso-contours of streamwise velocity fluctuations conditionally averaged in this manner. This particular ensemble average is for events that occur at $Re_\tau \approx 1400$ (corresponding to $x_{plate} = 1.2$ m) and the shear layers are detected at $z/\delta = 0.15$. This sequence shows time ranges for almost 10 boundary layer turnover times ($\Delta tU_\infty/\delta$) around the detected event. The sequence commences in figure 4(a) with a low and high-speed event that seem to span the logarithmic and wake regions. As the conditioned time approaches reference time (figures 4a-c), the low-speed region increasingly merges with the high-speed region (due to their mismatched convection velocities) giving rise to the sharp detected shear layer at the reference time (figure 4c). Associated with this process, the high-speed region appears to be pushed further from the wall. Though the shear layer formation mechanism seems apparent in figure 4, we should remain cautious of inferring complex three-dimensional turbulence structure from two-dimensional planar PIV slices. For example, the apparent shear layer formation observed in the sequence shown in figure 4 could also be explained by a streak and streamwise vortex structure, that increasingly penetrates our observation plane in time due to meandering (Kevin *et al.*, 2019). Temporally resolved DNS fields or tomographic PIV of an evolving turbulent boundary layer are necessary to show a detailed three-dimensional view of these structures.

Figure 5 shows an example of an interaction between low- and high-speed regions after the formation of a shear layer over a time evolution of 8 boundary layer turnover times. The sequence starts with a downstream low-speed region marked L1 which interacts with an upstream high-speed region, creating an inclined shear layer along with the interface due to the mismatched convection velocity, as observed in figures 4(a-b). Following this event, the local inclination angle along the interface (marked with a circle) changes due to the fact that L1 tends to kink upward (figure 5b), and eventually causes the subsequent roll-up creating a spanwise vortex feature as shown in figures 5(c-d). This development could be considered as a vortical motion which not only causes the L1 region to migrate away from the wall but also entrains the associated high-speed region towards the wall. Hence, the sequence may suggest that as the shear layer evolves in time, a local instability along the interface leads to a roll-up motion (such an observation would be in close agreement with earlier flow visualisation studies by Corino & Brodkey, 1969). Similar instantaneous sequences are frequently observed over a Reynolds number range $1000 < Re_\tau < 3000$ (not shown here for brevity). A similar observation of shear layer roll-up and associated ejection event has been recently reported in the numerical studies of Goudar *et al.* (2016). They also observed that the shearing process is associated with roll-up in the spanwise direction. Many of our instantaneous examples suggest that the low-speed region is not necessarily ejected all the way to the edge of a turbulent boundary layer, nor is the high-speed region necessarily entrained all the way to the wall. It is more likely that a number of these interactions, at numerous hierarchical scales, exist between the wall and the layer edge. However, the interaction between the low- and high-speed regions leading to the development of vortical motions is prevalently observed throughout our datasets.

On the basis of the above observations, we now discuss a simplified model that embodies key aspects of the evolution and interaction of low- and high-speed regions in relation to the temporal evolution of shear layers. Figure 6, which is in the wind tunnel frame of reference, shows that, on average, shear layers are generated when a coherent patch of positive u with an average convection velocity

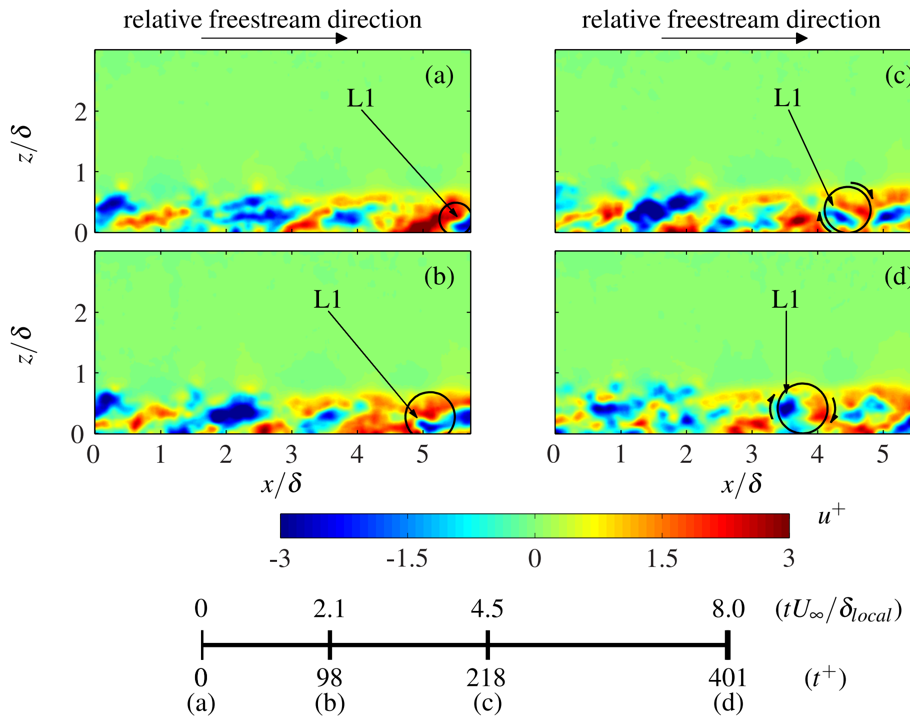

Figure 5. A sequence of events in u^+ fields after the formation of a shear layer over $1000 < Re_\tau < 1400$ ($0.6 < x_{plate}$(m) $<$ 1.2). Total duration of the sequence is approximately $t^+ \approx 400$ ($tU_{plate}/\delta_{local} \approx 8$). (a-d) indicate various stages of evolution.

higher than the local mean flow velocity approaches on a region of negative u (moving, on average, slower than the local mean). During the lifetime of these shear layers formed between these two interaction regions, the difference in the convection velocity remains distinct, such that the high-speed region over-runs the low-speed region. This results in stretching and subsequent roll-up of the shear layer. At this stage, the current observation is based on two-dimensional PIV data ($x-z$ plane) of evolving turbulent boundary layers and does not fully resolve all the effects of dynamic interaction including in the spanwise direction. In reality, we will also expect spanwise motions associated with these regions and interactions. Volumetric time-resolved DNS data or tomographic PIV could provide important additional insight in this regards. However, this conceptual scenario provides a perspective on the dynamic interactions of large-scale flow regions. The next challenge is to reconcile or incorporate this dynamic scenario into existing kinematic models such as the attached eddy or hairpin packet models.

Conclusions

A stationary time-resolved PIV system is used to probe the evolution of a turbulent boundary layer on a flat plate as it is towed through the field of view. The large-scale features are tracked and observed for their dynamics and evolution through this unique frame of reference. The results show that there is a clear difference in the convection velocities of low- and high-speed regions. This pronounced mismatch in convection speed allows the high- and low-speed regions to catch up to each other, causing an interaction that is associated with shear layer formation. This dynamical behaviour is not only observed instantaneously but also appears statistically in conditionally averaged time sequences. A roll-up mechanism appears to follow this shear layer formation.

A conceptual scenario is discussed to summarise the formation and time evolution of internal shear layers associated with low- and high-speed regions. Potentially, the dynamic interactions described in the scenario could be used to develop existing kinematic models.

REFERENCES

Adrian, R. J., Meinhart, C. D. & Tomkins, C. D. 2000 Vortex organization in the outer region of the turbulent boundary layer. *Journal of Fluid Mechanics* **422**, 1–54.

del Álamo, J.C. & Jiménez, J. 2009 Estimation of turbulent convection velocities and corrections to Taylor's approximation. *Journal of Fluid Mechanics* **640**, 5–26.

Christensen, K. T. & Adrian, R. J. 2001 Statistical evidence of hairpin vortex packets in wall turbulence. *Journal of Fluid Mechanics* **431**, 433–443.

Chung, D., Matheou, G. & Teixeira, J. 2012 Steady-state large-eddy simulations to study the stratocumulus to shallow cumulus cloud transition. *Journal of The Atmospheric Sciences* **69**, 3264–3276.

Corino, E. R. & Brodkey, R. S. 1969 A visual investigation of the wall region in turbulent flow. *Journal of Fluid Mechanics* **37**, 1–30.

Gao, Q., Ortiz-Dueñas, C. & Longmire, E. K. 2011 Analysis of vortex populations in turbulent wall-bounded flows. *Journal of Fluid Mechanics* **678**, 87–123.

Goudar, M. V., Breugem, W. P. & Elsinga, G. E. 2016 Autogeneration in wall turbulence by the interaction of weak eddies. *Physics of Fluids* **28** (3), 035111.

Hutchins, N. & Marusic, I. 2007 Evidence of very long meandering features in the logarithmic region of turbulent boundary layers. *Journal of Fluid Mechanics* **579**, 1–28.

Hutchins, N., Monty, J.P., Ganapathisubramani, B., Ng, H.C.H. & Marusic, I. 2011 Three-dimensional conditional structure of a high-Reynolds-number turbulent

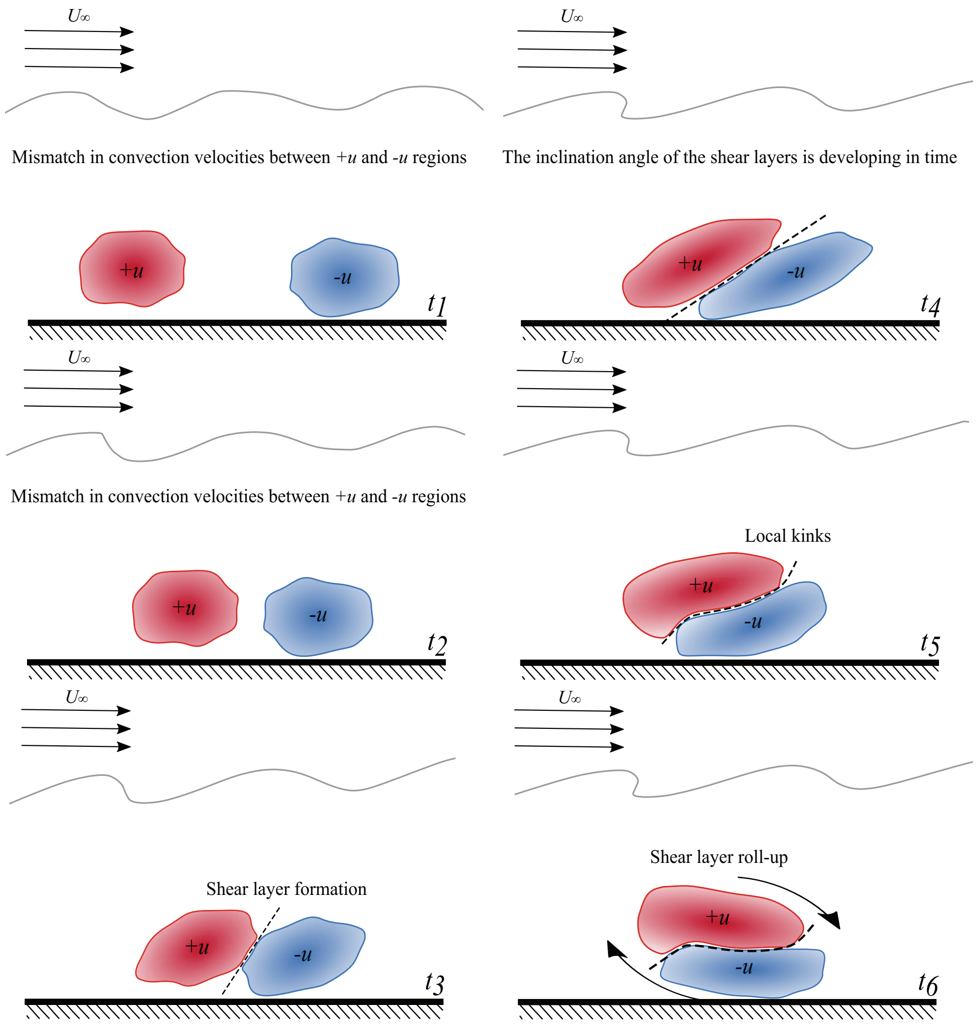

Figure 6. Schematic representation of the temporal evolution of high shear events described using low and high-speed regions. Flow is from left to right and advancing time is indicated by t_{1-6}

boundary layer. *Journal of Fluid Mechanics* **673**, 255–285.

Johansson, A. V., Alfredsson, P. H. & Kim, J. 1991 Evolution and dynamics of shear-layer structures in near-wall turbulence. *Journal of Fluid Mechanics* **224**, 579–599.

de Kat, R. & Ganapathisubramani, B. 2015 Convection of momentum transport events in a turbulent boundary layer. In *Proceedings of the International Symposium on Turbulence and Shear Flow Phenomena, TSFP-9, The University of Melbourne, Melbourne, Paper 4A-4*.

Kevin, Monty, J. & Hutchins, N. 2019 Turbulent structures in a statistically three-dimensional boundary layer. *Journal of Fluid Mechanics* **859**, 543–565.

Kim, H. T., Kline, S.J. & Reynolds, W.C. 1971 The production of turbulence near a smooth wall in a turbulent boundary layer. *Journal of Fluid Mechanics* **50**, 133–160.

Kline, S.J., Reynolds, W.C., Shrub, F.A. & Rundstadler, P.W. 1967 The structure of turbulent boundary layers. *Journal of Fluid Mechanics* **30**, 741–773.

Krogstad, P. A., Kaspersen, J. H. & Rimestad, S. 1998 Convection velocities in a turbulent boundary layer. *Physics of Fluids* **10**, 949–957.

Lee, J., Lee, J. H., Choi, J. I. & Sung, H. J. 2014*a* Spatial organization of large- and very-large-scale motion in a turbulent channel flow. *Journal of Fluid Mechanics* **749**, 818–840.

Lee, J. H. 2017 Evolution of canonical turbulent boundary layers. Ph.D. thesis, The University of Melbourne.

Lee, J. H., Kwon, Y. S., Monty, J. P. & Hutchins, N. 2014*b* Time-resolved PIV measurement of a developing zero pressure gradient turbulent boundary layer. In *Proc. 18th Australasian Fluid Mech. Conference*.

Lozano-Durán, A. & Jiménez, J. 2014 Time-resolved evolution of coherent structures in turbulent channels: characterization of eddies and cascades. *Journal of Fluid Mechanics* **759**, 432–471.

Monty, J. P. & Chong, M. S. 2009 Turbulent channel flow : comparison of streamwise velocity data from experiments and direct numerical simulation. *Journal of Fluid Mechanics* **633**, 461–474.

Robinson, S.K. 1991 Coherent motions in the turbulent boundary layer. *Annu. Rev. Fluid Mech.* **23**, 601–639.

de Silva, C. M., Hutchins, N. & Marusic, I. 2016 Uniform momentum zones in turbulent boundary layers. *Journal of Fluid Mechanics* **786**, 309–331.

Willmarth, W. W. & Lu, S. S. 1972 Structure of the reynolds stress near the wall. *Journal of Fluid Mechanics* **55**, 65–92.